ACS Photonics

pubs.acs.org/journal/apchd5

Article

Single-Pixel Multimode Fiber Spectrometer via Wavefront Shaping

Sahin Kurekci,* S. Suleyman Kahraman, and Emre Yuce

Cite This: *ACS Photonics* 2023, 10, 2488–2493

Read Online

ACCESS | Metrics & More | Article Recommendations | Supporting Information

ABSTRACT: When light passes through a multimode fiber, two-dimensional random intensity patterns are formed due to complex interference within the fiber. The extreme sensitivity of speckle patterns to the frequency of light paved the way for high-resolution multimode fiber spectrometers. However, this approach requires expensive IR cameras and impedes the integration of spectrometers on-chip. In this study, we propose a single-pixel multimode fiber spectrometer by exploiting wavefront shaping. The input light is structured with the help of a spatial light modulator, and optimal phase masks, focusing light at the distal end of the fiber, are stored for each wavelength. Variation of the intensity in the focused region is recorded by scanning all wavelengths under fixed optimal masks. Based on the intensity measurements, we show that an arbitrary input spectrum having two wavelengths 20 pm apart from each other can be reconstructed successfully (with a reconstruction error of ~3%) in the near-infrared regime, corresponding to a resolving power of $R \approx 10^5$. We also demonstrate the reconstruction of broadband continuous spectra with varying bandwidths. With the installation of a single-pixel detector, our method provides compact detection and a lower budget alternative to conventional systems, with potential promise to operate at low-signal levels.

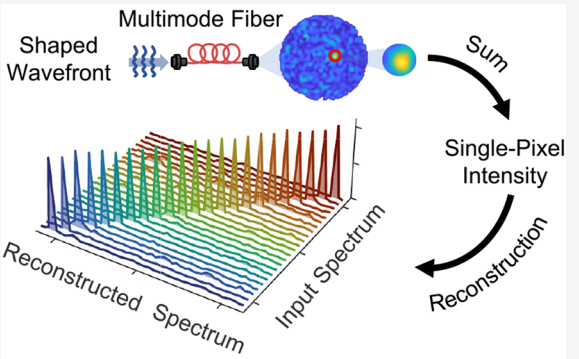

KEYWORDS: *spectrometer, single-pixel, multimode fiber, wavefront shaping, fiber optics, spatial light modulator*

1. INTRODUCTION

Spectrometers achieve spectral-to-spatial mapping, which allows spectral decomposition of the input light. Conventional spectrometers use dispersive media such as gratings or prisms, and they can achieve resolving powers around $R < 10^4$ and can reach up to $R < 10^5$ only with the installation of complex triple-grating systems (the spectral resolution is $\delta\lambda = \lambda_0/R$, where λ_0 is the operating wavelength). However, such spectrometers generally require moving parts (gratings and mirrors) and a line array detector for scanning whole wavelengths of interest. Moreover, the inverse proportionality between spectral resolution and optical path length leads to bulky systems when high-resolution is demanded. The fundamental need for high resolution spectral analysis in various lines of research and applications triggers new concepts that are built on the basis of scattering media, which create complex spatial intensity distributions (speckle patterns) captured on a multipixel detector such as a charged couple device (CCD) or a focal plane array (FPA).[1−16] In such systems, wavelengths experience different propagation constants inside the scattering medium, thus forming distinct spatial intensity profiles on the detector, which provide the required one-to-one spectral-to-spatial mapping. Before the use of the spectrometer, a calibration matrix is measured by scanning all wavelengths in the operational range, and storing the corresponding speckle patterns. The calibration matrix is then utilized to reconstruct an arbitrary input spectrum based on the measured intensity distribution.

Among all scattering-based systems, the multimode fiber spectrometers[5−8] have been particularly attractive by offering high resolutions with reduced scattering losses (keeping the light collimated inside the fiber and preventing scattering to higher angles). Since fibers can be wrapped, higher spectral resolution can be achieved without enlarging the system. It was shown in ref 7 that high resolving powers $R > 10^6$ in the near-infrared regime are possible with fibers of 100 m length. Yet the signal-to-noise ratio (SNR) is the main limiting factor for the resolution at low signal levels and increased fiber length.[17]

Single pixel detection together with compressed sensing[18−20] have been revolutionizing imaging methods. Surprisingly, the penetration of this method in spectroscopy has been very limited due to mechanical resolution limits; that is, due to the requirement of rotating optics such as gratings or mirrors in single-pixel spectroscopic analysis.[21] The single-pixel imaging (SPI) systems are compact systems based on the use of a spatial light modulator (SLM) and a single-pixel

Received: November 12, 2022
Published: July 13, 2023

detector, and employing the SPI method is particularly useful when working in the infrared regime since CCDs and FPAs get extremely expensive at longer wavelengths.[22]

In this article, we develop a high-resolution single-pixel multimode fiber spectrometer and demonstrate its ability to reconstruct arbitrary spectra. The single-pixel detection is achieved by focusing light on a selected target region of a focal plane array, which is employed as a bucket detector. The input wavefronts are structured using a spatial light modulator, which provides distinct output intensities at the detector.[23−27] The intensity variations at the target position as a function of input wavelength are used to reconstruct the spectra at a resolution of 20 pm. Replacing an FPA with a single-pixel detector reduces the cost in infrared applications enormously, and it may also provide a new method for on-chip compressed imaging, which is brought by the compact size of a single-pixel spectrometer. Furthermore, the increased intensity at the focused point has the potential to increase the performance of the multimode fiber spectrometer in low-signal regimes.

2. RESULTS AND DISCUSSION

The spectrometer is built based on the system given in Figure 1. The light is phase-modulated via an SLM and focused on the distal end of a 20-m-long multimode fiber. The intensity at the focus spot is then integrated to reconstruct the input spectrum from single-pixel data. Since the whole spectrometer is built upon the intensity measurements of the target region, which effectively covers an area around 0.07 mm^2, the bucket detector can safely be replaced with commercial photodiodes which generally have active areas larger than the size of our target region.[28]

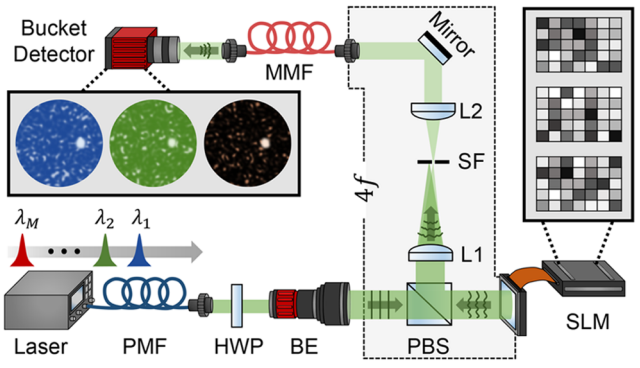

Figure 1. Schematic of the setup. The intensity of the input wavelengths provided by a tunable laser is optimized at the end of a 20 m long multimode fiber by using a spatial light modulator. Unique SLM patterns are used to focus on distinct wavelengths. L: lens, PMF: polarization maintaining fiber, HWP: half-wave plate, BE: beam expander, PBS: polarizing beam splitter, SLM: spatial light modulator, SF: spatial filter, MMF: multimode fiber.

In order to calibrate the spectrometer, we have modified the calibration process in ref 6 for an SLM-based single-pixel system as depicted in Figure 2. We represent the input spectrum of a single wavelength λ_i as a unit vector:

$$\mathbf{S_i} = [\lambda_1,\ \lambda_2,\ ...,\ \lambda_M]^T \tag{1}$$

where all the elements except $\lambda_i = 1$ are set to zero (T is the transpose operator). All M input wavelengths within the scope of the operating range of the spectrometer are modulated by the SLM, and the intensities are optimized on the target region of the detector. The optimized SLM phase masks, ϕ_i (i = 1, 2, ..., M), are stored. Once the optimization process is completed, the target region intensities of individual wavelengths are measured under all recorded SLM patterns, and the intensity values are then integrated into a single numerical value. Throughout the text, $I_{\lambda_i}^{\phi_j}$ denotes the integrated intensity of the target region under input wavelength λ_i and optimized SLM pattern ϕ_j. For each wavelength λ_i (or spectrum vector $\mathbf{S_i}$), a corresponding intensity vector as a function of SLM phase mask ϕ is created:

$$\mathbf{I_i} = [I_{\lambda_i}^{\phi_1},\ I_{\lambda_i}^{\phi_2},\ ...,\ I_{\lambda_i}^{\phi_M}]^T \tag{2}$$

The intensity vectors are then combined into a single $M \times M$ matrix $\mathbf{T}$, which is called the calibration matrix, whose rows can be used as a measure of the system response to wavelength variations. With the implementation of advanced wavefront optimization methods, it is possible to focus light in milliseconds[29] and complete the calibration of the spectrometer in less than a few minutes for many practical spectroscopy applications.

The entries sitting in the main diagonal of the calibration matrix are expected to have the highest numerical values in their row and column, since they correspond to the perfect match between the input wavelength and the optimized SLM pattern. In the off-diagonal entries, wavelength and the optimized phase mask mismatch, and as a result, the integrated intensity drops for steps out of the diagonal. More contrast between the diagonal and off-diagonal entries can be produced when the light is sharply focused on the detector. In this case, the spectrometer is expected to exhibit more sensitivity to wavelength variations and thus to have a higher resolution. The sharpness of the focus can be controlled by involving a measure of merit (such as the enhancement factor) during the optimization. In our experiments, we measured an average enhancement around $\eta \approx 70$, which is approximately 40% below the theoretical maximum value.[26]

The calibration process of the spectrometer can be modeled mathematically as a set of linear propagations where the inputs are the spectrum vectors $\mathbf{S_i}$, outputs are the intensity vectors $\mathbf{I_i}$, and the propagation operator is the calibration matrix $\mathbf{T}$,

$$\mathbf{T}\cdot\mathbf{S_i} = \mathbf{I_i} \tag{3}$$

To test the performance of the spectrometer, an unknown spectrum $\mathbf{S_u^{probe}}$ is sent through the system, and the corresponding intensity vector $\mathbf{I_u}$ is captured. By inverting eq 3, we obtain the reconstructed spectrum vector $\mathbf{S_u^{reconstructed}}$ based on the calibration data and the measured intensity:

$$\mathbf{S_u^{reconstructed}} = \mathbf{T^{-1}}\cdot\mathbf{I_u} \tag{4}$$

The performance of the spectrometer is measured by comparing the reconstructed spectrum to the actual probe spectrum, where the comparison is done by calculating the root-mean-square error:

$$\mu = \sqrt{\frac{1}{M}[\mathbf{S_{probe}} - \mathbf{S_{reconstructed}}]^2} \tag{5}$$

Using the calibration process explained in Figure 2, we have calibrated our system with 50 wavelengths around the central wavelength 1550 nm (from 1549.75 to 1550.24 nm) with 10 pm step size between consecutive wavelengths. After the calibration matrix is obtained and stored, individual wave-

https://doi.org/10.1021/acsphotonics.2c01766
ACS Photonics 2023, 10, 2488−2493

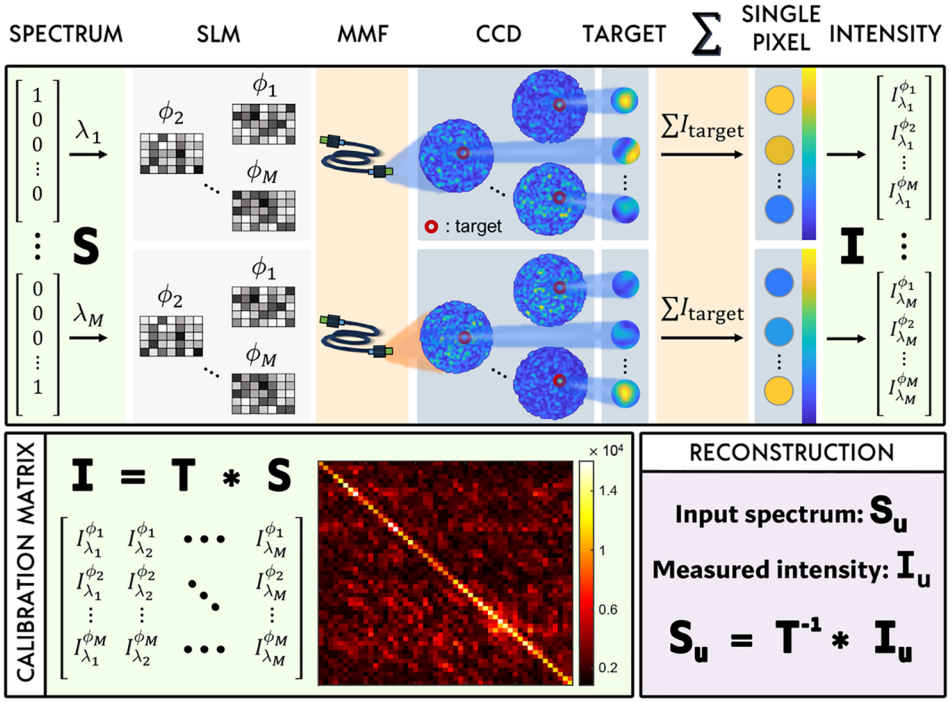

Figure 2. Schematic explanation of the calibration and reconstruction. The upper rectangle illustrates the process used to obtain the calibration matrix **T**. The heatmap of the 50 × 50 calibration matrix obtained in the experiment is shown inside the bottom-left rectangle. Using the inverse of the calibration matrix, an unknown input spectrum can be reconstructed as formulated in the bottom-right corner. The asterisk operator (*) denotes matrix multiplication.

lengths are sent through the system, and measured intensities are plugged in eq 4. The reconstructed spectrum vectors of individual wavelengths in the spectral range are plotted in Figure 3(a). Since optical signals of different wavelengths do not interfere, an arbitrary spectrum can be modeled with a tunable laser by creating the spectrum content separately and then superposing the measured intensities. In the mathematical formulation, we sum the individual intensity vectors and plug the resulting vector in eq 4 as the measured intensity. For two wavelengths 20 pm apart from each other, the spectrum reconstruction is shown in Figure 3(b). We show that a single-pixel spectrometer can resolve the spectral lines accurately and can reconstruct the unknown input spectrum with a reconstruction error $\mu = 0.0298$.

While the input light entering the system may consist of sparse wavelengths, it may also carry a broadband spectrum. In this case, we model the continuous broadband spectrum as a weighted combination of individual wavelengths. We discretize the broadband spectrum with 10 pm spacing, which is the step size between two consecutive wavelengths in our data set. To test the performance of the spectrometer, we modeled broadband Lorentzian beams of different bandwidths in the 490 pm spectral range from 1549.75 to 1550.24 nm. Each wavelength involved in the broadband signal is expected to contribute to the final intensity by its weight in the spectrum. Thus, the final intensity measured on the detector is found by superposing the individual intensity vectors scaled by the weight of the corresponding wavelength. The reconstruction results obtained from the final intensity vector for three Lorentzian beams centered at 1549.99 nm with 20, 100, and 200 pm bandwidths corresponding to ∼4%, ∼20%, and ∼40% of the total spectral range are plotted in Figure 3(c). It is observed that the reconstruction error increases with the bandwidth of the signal, reaching ∼6% ($\mu = 0.0569$) when ∼40% of the spectral range is covered in the bandwidth.

It is possible to reduce the spectrum reconstruction error of a multimode fiber based speckle spectrometer by suppressing the system noise using computational methods such as truncated inversion.[6] In this study, we show pure physical results solely based on intensity measurements without any computational aid. The computational manipulations should be handled carefully in a single-pixel spectrometer since (1) the number of data points are fewer compared to a speckle spectrometer which may immediately dismiss some methods, and (2) diagonal data are positively biased in the calibration matrix of the single-pixel spectrometer opposite the speckle spectrometer where the data are randomly distributed due to the nature of speckle images. A computational method preserving the diagonality of the calibration matrix and simultaneously respecting the correlation between the columns of **T** may be a good candidate for reducing the errors. Increasing the isolation of the system by stabilizing the multimode fiber is another way of suppressing the system noise.[8] In preferred cases, the isolation can be provided by replacing the multimode fiber with an integrated ridge waveguide, which is much less susceptible to environmental variations. With such improvements, we believe the single-pixel spectrometer will be able to go beyond the resolution limit of a speckle spectrometer, which is more affected by the detection noise.[17]

The single-pixel spectrometer may also be promising to operate better at low-signal regimes compared to a speckle-based spectrometer, which, however, needs further investigations. Specifically, parameters such as the number of calibrated wavelengths, the number of modes in the multimode fiber, and SLM insertion loss should be taken into

https://doi.org/10.1021/acsphotonics.2c01766
ACS Photonics 2023, 10, 2488−2493

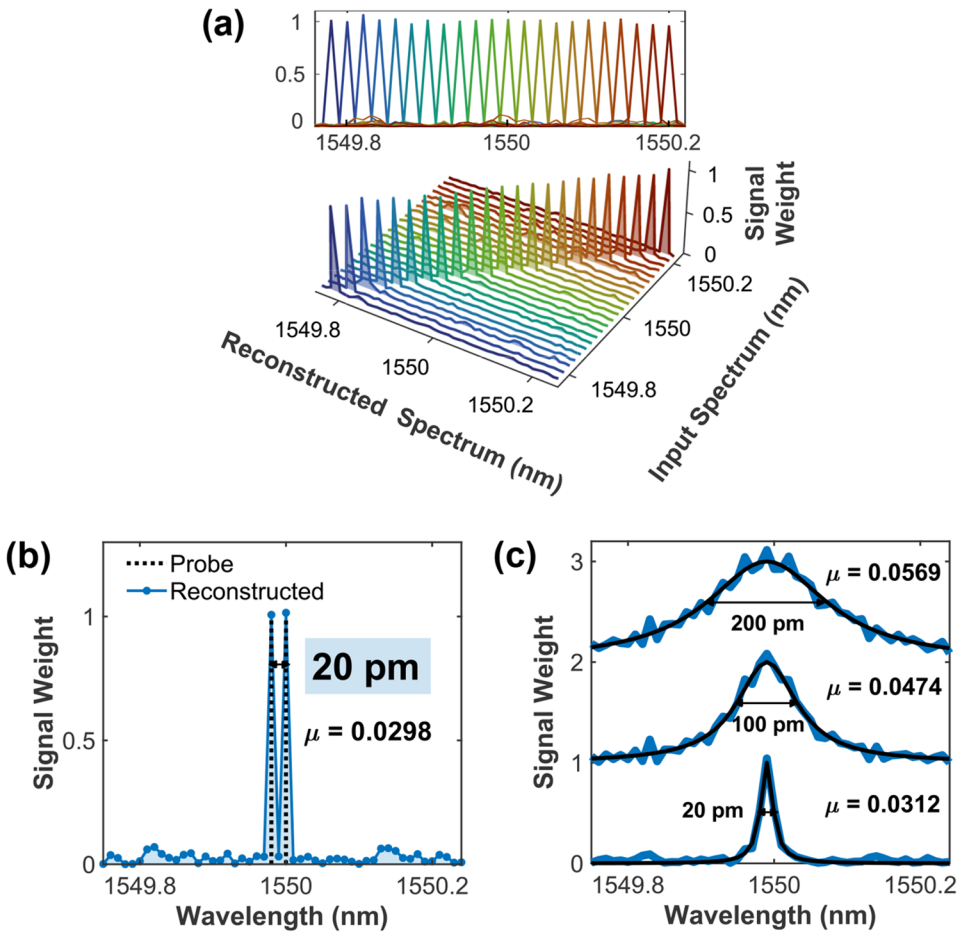

Figure 3. Performance of the spectrometer in reconstructing (a) individual wavelengths, (b) arbitrary spectra with two wavelengths, and (c) broadband Lorentzian spectra of various bandwidths.

consideration, and their effects on the improvement of signal-to-noise ratio should be studied. Among these parameters, the insertion loss of the SLM is expected to negatively affect the SNR of the system, especially at very low signal levels. The number of modes, on the other hand, can potentially enhance the SNR at the focused wavelength since a sharper focus can be obtained with a fiber supporting more modes, which, as a result, reduces the fraction of light falling on regions other than the target region. However, when other wavelengths are scanned (the wavelength is switched from the optimal wavelength for which the SLM is optimized), a high number of modes may lead to more light escaping to the outer regions. Therefore, the mutual effect of the number of modes and number of wavelengths on SNR may be intricate and requires thorough examination across different signal levels.

3. CONCLUSION

In summary, we have demonstrated a high-resolution, single-pixel, multimode fiber spectrometer employing wavefront shaping of light. The working principle of the spectrometer is based on the abrupt distortion of the focused intensity when the wavelength of the incoming light changes. However, the use of SLM may not be required to build such a system. Instead, controlled external perturbations can be used to create a calibration matrix whose columns or rows are distinctive enough to separate the wavelengths, which may lead to a similar system under specific arrangements. The use of SLM, on the other hand, may be potentially promising in breaking the low signal barrier of speckle spectrometers. The efforts regarding the miniaturized wavefront controllers can pave the way for simultaneous spectral reconstruction at low signal levels.[30−32]The proposed spectrometer is promising in developing applications across scattering media, and it offers replacing bulky, expensive cameras with a single-pixel detector to develop lower budget systems.

4. EXPERIMENTAL METHODS

The experimental setup is provided in Figure 1. A tunable laser operating around 1550 nm with a 38 nm tuning range is used for illuminating an SLM (HOLOEYE PLUTO-TELCO) with a 1920 × 1080 pixel screen resolution. The beam is expanded to cover the SLM screen, and a half-wave plate is used to control the incident polarization so that it matches the alignment direction of the liquid crystals inside the SLM. To avoid the contribution of the pixelated nature of the SLM on the measurements, a fixed blazed grating is kept on the SLM for all measurements and zeroth-order diffracted light is eliminated with a spatial filter.[33] The 20-m-long fiber we used in the setup has a 105 μm core diameter and 0.22 NA. The light focused at the distal end of the fiber covers 76 pixels on the chip of a 256 × 320 pixel resolution FPA detector. The cell size of the detector is 30 μm × 30 μm. A continuous sequential algorithm[34] is used in the modulation steps where the SLM is

https://doi.org/10.1021/acsphotonics.2c01766
ACS Photonics 2023, 10, 2488−2493

divided into 144 superpixels of a size of 16 × 9 and four phase steps between 0 and 2π are scanned through each superpixel.

■ ASSOCIATED CONTENT

Supporting Information

The Supporting Information is available free of charge at https://pubs.acs.org/doi/10.1021/acsphotonics.2c01766.

Calibration and test images of the single-pixel spectrometer system (ZIP)

■ AUTHOR INFORMATION

Corresponding Author

Sahin Kurekci − *Programmable Photonics Group, Department of Physics, Middle East Technical University, Ankara 06800, Turkey;* orcid.org/0000-0002-0190-3442; Email: kurekci@metu.edu.tr

Authors

S. Suleyman Kahraman − *Programmable Photonics Group, Department of Physics, Middle East Technical University, Ankara 06800, Turkey; Caltech Optical Imaging Laboratory, Andrew and Peggy Cherng Department of Medical Engineering, Department of Electrical Engineering, California Institute of Technology, Pasadena, California 91125, United States*

Emre Yuce − *Programmable Photonics Group, Department of Physics, Middle East Technical University, Ankara 06800, Turkey;* orcid.org/0000-0001-7808-1988

Complete contact information is available at: https://pubs.acs.org/10.1021/acsphotonics.2c01766

Funding

This work is financially supported by the Technological and Research Council of Türkiye (TÜBİTAK), grant 118M199, grant 2211-A, and Turkish Academy of Sciences Outstanding Young Scientists Award Program (TÜBA-GEBİP)

Notes

The authors declare the following competing financial interest(s): Two patents (PCT Patent Application No: PCT/TR2021/051613 pending, PCT/TR2021/051305 pending) on the use of spatial light modulators in building spectrometers have been filed by Middle East Technical University with E.Y. and S.K. as inventors. All other authors declare they have no competing interests.

■ ACKNOWLEDGMENTS

The authors thank Alpan Bek for helpful discussions.

■ REFERENCES

(1) Yüce, E.; Kürekci, S. Compact Holographic SLM Spectrometer. Pending-patent, Turkish Patent and Trademark Office application number: 2020/22701. International application number: PCT/TR2021/051613, 2020.

(2) Xu, Z.; Wang, Z.; Sullivan, M. E.; Brady, D. J.; Foulger, S. H.; Adibi, A. Multimodal multiplex spectroscopy using photonic crystals. *Opt. Express* **2003**, *11*, 2126−2133.

(3) Redding, B.; Liew, S. F.; Sarma, R.; Cao, H. Compact spectrometer based on a disordered photonic chip. *Nat. Photonics* **2013**, *7*, 746−751.

(4) Kohlgraf-Owens, T. W.; Dogariu, A. Transmission matrices of random media: means for spectral polarimetric measurements. *Opt. Lett.* **2010**, *35*, 2236−2238.

(5) Yüce, E.; Kürekci, S. Interference-Based Spectrometer With Multimode Medium. Pending-patent, International application number: PCT/TR2021/051305, 2021.

(6) Redding, B.; Popoff, S. M.; Cao, H. All-fiber spectrometer based on speckle pattern reconstruction. *Opt. Express* **2013**, *21*, 6584−6600.

(7) Redding, B.; Alam, M.; Seifert, M.; Cao, H. High-resolution and broadband all-fiber spectrometers. *Optica* **2014**, *1*, 175−180.

(8) Wan, N. H.; Meng, F.; Schröder, T.; Shiue, R.-J.; Chen, E. H.; Englund, D. High-resolution optical spectroscopy using multimode interference in a compact tapered fibre. *Nat. Commun.* **2015**, *6*, 7762.

(9) Wan, Y.; Wang, S.; Fan, X.; Zhang, Z.; He, Z. High-resolution wavemeter using Rayleigh speckle obtained by optical time domain reflectometry. *Opt. Lett.* **2020**, *45*, 799−802.

(10) Wan, Y.; Fan, X.; Wang, S.; Zhang, Z.; Xu, B.; He, Z. Rayleigh speckle-based wavemeter with high dynamic range and fast reference speckle establishment process assisted by optical frequency combs. *Opt. Lett.* **2021**, *46*, 1241−1244.

(11) Bruce, G. D.; O'Donnell, L.; Chen, M.; Facchin, M.; Dholakia, K. Femtometer-resolved simultaneous measurement of multiple laser wavelengths in a speckle wavemeter. *Opt. Lett.* **2020**, *45*, 1926−1929.

(12) Hartmann, W.; Varytis, P.; Gehring, H.; Walter, N.; Beutel, F.; Busch, K.; Pernice, W. Broadband Spectrometer with Single-Photon Sensitivity Exploiting Tailored Disorder. *Nano Lett.* **2020**, *20*, 2625−2631. PMID: 32160472

(13) Yi, D.; Zhang, Y.; Wu, X.; Tsang, H. K. Integrated Multimode Waveguide With Photonic Lantern for Speckle Spectroscopy. *IEEE J. Quantum Electron.* **2021**, *57*, 1−8.

(14) Zhang, Z.; Li, Y.; Wang, Y.; Yu, Z.; Sun, X.; Tsang, H. K. Compact High Resolution Speckle Spectrometer by Using Linear Coherent Integrated Network on Silicon Nitride Platform at 776 nm. *Laser & Photonics Reviews* **2021**, *15*, 2100039.

(15) Meng, Z.; Li, J.; Yin, C.; Zhang, T.; Yu, Z.; Tang, M.; Tong, W.; Xu, K. Multimode fiber spectrometer with scalable bandwidth using space-division multiplexing. *AIP Advances* **2019**, *9*, 015004.

(16) Falak, P. L.; Sun, Q.; Vettenburg, T.; Lee, T.; Phillips, D. B.; Brambilla, G.; Beresna, M. Femtosecond laser written scattering chip for high-resolution low-cost reconstructive spectrometry. *Photonic Instrumentation Engineering* **2022**, *IX*, 120080E.

(17) Cao, H. Perspective on speckle spectrometers. *Journal of Optics* **2017**, *19*, 060402.

(18) Takhar, D.; Laska, J. N.; Wakin, M. B.; Duarte, M. F.; Baron, D.; Sarvotham, S.; Kelly, K. F.; Baraniuk, R. G. A new compressive imaging camera architecture using optical-domain compression. *Proc. Computational Imaging IV* **2006**, *6065*, 43−52.

(19) Duarte, M. F.; Davenport, M. A.; Takbar, D.; Laska, J. N.; Sun, T.; Kelly, K. F.; Baraniuk, R. G. Single-pixel imaging via compressive sampling. *IEEE Signal Processing Magazine* **2008**, *25*, 83−91.

(20) Gattinger, P.; Zorin, I.; Rankl, C.; Brandstetter, M. Spectral-Coding-Based Compressive Single-Pixel NIR Spectroscopy in the Sub-Millisecond Regime. *Sensors* **2021**, *21*, 5563.

(21) Chen, M.; Xie, S.; Wu, H.; Takahashi, S.; Matsumoto, H.; Takamasu, K. Spectroscopic interferometer with a large length range by rotating diffraction grating. *Opt. Express* **2019**, *27*, 10553−10563.

(22) Edgar, M. P.; Gibson, G. M.; Padgett, M. J. Principles and prospects for single-pixel imaging. *Nat. Photonics* **2019**, *13*, 13−20.

(23) Vellekoop, I. M.; Mosk, A. P. Focusing coherent light through opaque strongly scattering media. *Opt. Lett.* **2007**, *32*, 2309−2311.

(24) Vellekoop, I. M.; van Putten, E. G.; Lagendijk, A.; Mosk, A. P. Demixing light paths inside disordered metamaterials. *Opt. Express* **2008**, *16*, 67−80.

(25) Mosk, A. P.; Lagendijk, A.; Lerosey, G.; Fink, M. Controlling waves in space and time for imaging and focusing in complex media. *Nat. Photonics* **2012**, *6*, 283−292.

(26) Vellekoop, I. M. Feedback-based wavefront shaping. *Opt. Express* **2015**, *23*, 12189−12206.

(27) Horstmeyer, R.; Ruan, H.; Yang, C. Guidestar-assisted wavefront-shaping methods for focusing light into biological tissue. *Nat. Photonics* **2015**, *9*, 563−571.

(28) Donati, S. *Photodetectors: devices, circuits and applications*, 2nd ed.; Wiley-IEEE Press, 2021.
(29) Xia, M.; Li, D.; Wang, L.; Wang, D. Fast optical wavefront engineering for controlling light propagation in dynamic turbid media. *Journal of Innovative Optical Health Sciences* **2019**, *12*, 1930007.
(30) Wei, Q.; Huang, L.; Zentgraf, T.; Wang, Y. Optical wavefront shaping based on functional metasurfaces. *Nanophotonics* **2020**, *9*, 987−1002.
(31) Guo, Y.; Guo, Y.; Li, C.; Zhang, H.; Zhou, X.; Zhang, L. Integrated Optical Phased Arrays for Beam Forming and Steering. *Applied Sciences* **2021**, *11*, 4017.
(32) Deng, L.; Xu, Y.; Jin, R.; Cai, Z.; Liu, Y. On-Demand Mode Conversion and Wavefront Shaping via On-Chip Metasurfaces. *Advanced Optical Materials* **2022**, *10*, 2200910.
(33) Qi, Y.; Chang, C.; Xia, J. Speckleless holographic display by complex modulation based on double-phase method. *Opt. Express* **2016**, *24*, 30368.
(34) Vellekoop, I. M.; Mosk, A. P. Phase control algorithms for focusing light through turbid media. *Opt. Commun.* **2008**, *281*, 3071−3080.

https://doi.org/10.1021/acsphotonics.2c01766
ACS Photonics 2023, 10, 2488−2493